The EMBO Journal (2009) 28, 602–613 | © 2009 European Molecular Biology Organization | All Rights Reserved 0261-4189/09
www.embojournal.org

THE EMBO JOURNAL

Spatially and kinetically resolved changes in the conformational dynamics of the Hsp90 chaperone machine

Christian Graf, Marta Stankiewicz, Günter Kramer and Matthias P Mayer*

Zentrum für Molekulare Biologie der Universität Heidelberg (ZMBH), DKFZ-ZMBH Alliance, Heidelberg, Germany

The highly conserved 90 kDa heat shock protein (Hsp90) chaperones use ATP to regulate the stability and activity of many signalling molecules like protein kinases and transcription factors. Studies using crystallography, electron microscopy and small-angle X-ray scattering yielded controversial results for the conformational states that these dimeric multidomain proteins assume while progressing through the ATPase cycle. To better understand the molecular mechanism of Hsp90 proteins, we studied the conformational dynamics of the *Escherichia coli* homologue HtpG in solution using amide hydrogen exchange mass spectrometry (HX-MS) and fluorescence spectroscopy. A conformation-sensitive fluorescent probe allowed to elucidate the ATPase cycle of HtpG. Continuous-labelling and pulse-labelling HX-MS experiments revealed major ATP-induced conformational changes throughout the protein that do not occur simultaneously, but progress surprisingly slow from the immediate nucleotide-binding site towards the N terminus and the middle domain. The conversion between the different conformational states is rate limiting for ATP hydrolysis, and the nucleotide-coordinating residue, Glu34, is important for the rate constant of conversion. Our findings, for the first time, allow to kinetically resolve changes in the conformational dynamics of individual structural elements of Hsp90.

The EMBO Journal (2009) **28,** 602–613. doi:10.1038/emboj.2008.306; Published online 22 January 2009
Subject Categories: signal transduction; structural biology
Keywords: amide hydrogen exchange; conformational dynamics; kinetics; mass spectrometry; molecular chaperone

Introduction

The 90 kDa heat shock proteins (Hsp90) are essential chaperones in all eukaryotes. Assisted by a large number of cochaperones, Hsp90s control the stability and activity of some 200 client proteins, which are mostly regulatory components of signal transduction pathways, such as receptors, protein kinases and transcription factors (Mayer and Bukau, 1999; Wegele *et al*, 2004; Pearl *et al*, 2008).

The Hsp90 family of proteins is highly conserved, for example, *Escherichia coli* and human members share 40% sequence identity. Hsp90 proteins consist of an N-terminal nucleotide-binding domain (NBD), a middle domain (MD) and a C-terminal dimerization domain (DD). Structural information exists for both individual domains and nearly full-length Hsp90 variants in complex with different nucleotides and inhibitors (Stebbins *et al*, 1997; Prodromou *et al*, 1997b; Meyer *et al*, 2003; Harris *et al*, 2004; Huai *et al*, 2005; Ali *et al*, 2006 reviewed in Pearl and Prodromou, 2006; Shiau *et al*, 2006). ATP binding and hydrolysis is essential for the chaperone activity of Hsp90 *in vivo* (Obermann *et al*, 1998; Panaretou *et al*, 1998).

On the basis of the structure of the related GHKL-ATPase DNA gyrase B and biochemical data, the ATPase cycle of Hsp90 is proposed to involve several conformational changes. These include an ATP-dependent docking of NBD and MD of the same monomer, and a dimerization of the two NBDs in the Hsp90 dimer, which results in a ring-shaped structure (Pearl and Prodromou, 2002; Richter *et al*, 2002; Immormino *et al*, 2004; Ali *et al*, 2006). The crystal structure of yeast Hsp90 in complex with AMPPNP and Sba1 and recent biochemical studies are consistent with this proposed catalytic mechanism (Ali *et al*, 2006; Cunningham *et al*, 2008; Vaughan *et al*, 2009). However, a crystallographic and electron microscopy study on HtpG presented evidence for strikingly different conformations depending on the presence or absence of AMPPNP or ADP, none of which fits the conformation proposed to be necessary for catalysis (Shiau *et al*, 2006). In this publication, a highly compact ADP-bound state was proposed, which could, however, not be observed by small-angle X-ray scattering (SAXS) in another investigation (Krukenberg *et al*, 2008). The SAXS data of HtpG were interpreted in terms of multiple coexisting conformations.

To analyse the conformational dynamics of Hsp90 during progression through the ATPase cycle, we employed amide hydrogen-^{1}H/^{2}H-exchange (HX) mass spectrometry (MS) and fluorescence spectroscopy. We focused on the bacterial Hsp90 homologue HtpG because it is the most simple representative of the Hsp90 family and does not seem to be regulated by cochaperones. In this study, we resolved the changes in conformational dynamics in space and time. We show that ATP binding induces a series of conformational changes to attain a tense pre-hydrolysis state with greatly reduced secondary structure flexibility.

Results

Deuteron incorporation into full-length HtpG

To analyse the conformational flexibility of HtpG, we performed continuous-labelling HX-MS experiments as

*Corresponding author: Zentrum für Molekulare Biologie der Universität Heidelberg (ZMBH), DKFZ-ZMBH Alliance, Im Neuenheimer Feld 282, 69120 Heidelberg, Germany.
Tel.: +49 6221 546829; Fax: +49 6221 545894;
E-mail: M.Mayer@zmbh.uni-heidelberg.de

Received: 30 October 2008; accepted: 22 December 2008; published online: 22 January 2009

described previously (Rist *et al*, 2003, 2006) and shown schematically in Figure 1A. With these experiments, global stability and different conformational states of a protein can be analysed.

Apo-HtpG exchanged about 38% of its exchangeable amide hydrogens within 10 s and about 60% within 1 h in D_2O (Figure 1B). Addition of ADP only induced a small protection (ca. 7 amide hydrogens). However, in the presence of ATP solvent, accessibility of HtpG was strongly reduced as compared with apo-HtpG, with almost 50 protected amide hydrogens. This protection slowly decreased to the level of the apo state by 1200 s (Figure 1B; for a detailed discussion see Supplementary data part 1). These data indicate that the HtpG state with least amide hydrogens accessible can only be reached through addition of ATP but not of ADP, which seems to be at odds with a structural study on HtpG (Shiau *et al*, 2006). However, these experiments do not exclude the alternative interpretation that the solvent protected ATP-induced state is a post-hydrolysis conformation. We considered this possibility because the generation of the ATP-induced protected state required a pre-incubation of HtpG with ATP that was much longer than we had expected for a protein with high nucleotide association rate constants (see below).

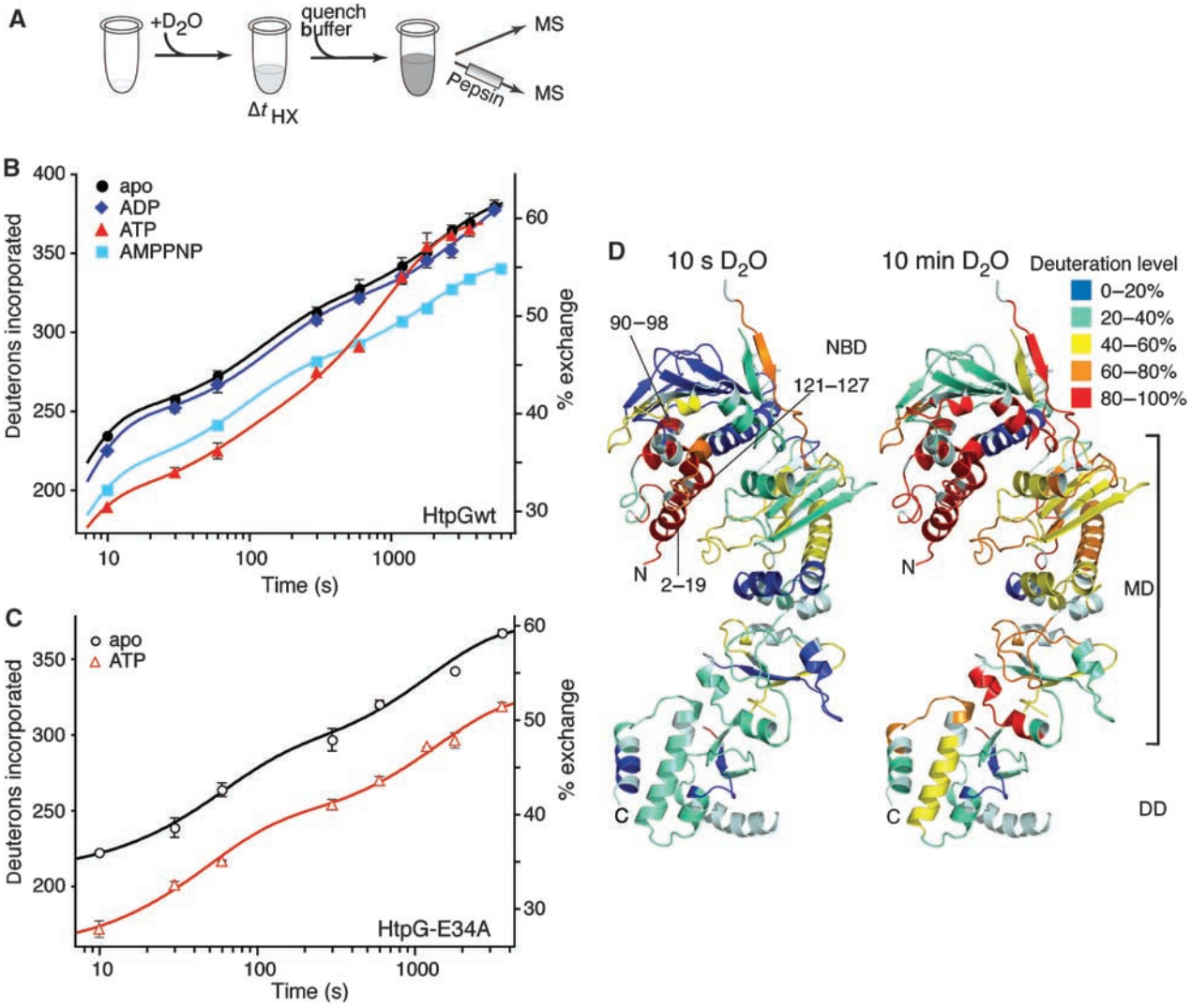

Figure 1 HX kinetics of the full-length HtpG and localization of fast and slow exchanging regions. (**A**) Scheme of the continuous labelling HX experiment. HX is initiated by diluting the equilibrated sample 1:20 into D_2O buffer (pD 7.4). After different incubation times at 30°C, temperature is lowered to 0°C and pH to 2.5 by addition of ice-cold phosphate buffer (quench buffer). The reaction is subsequently analysed by HPLC-MS. For the analysis of overall exchange rate constants (B, C) full-length proteins are desalted on a reversed-phase trap column and eluted over an analytical column into the mass spectrometer. For localization of fast and slow exchanging regions (D) peptic fragments of the protein are generated online by including a column with immobilized pepsin in front of the trap column. (**B**) Numbers of deuterons incorporated into full-length *E. coli* HtpG in the absence of nucleotides (black circles) and in the presence of ADP (blue diamonds), ATP (red triangles) and AMPPNP (cyan squares). The *y*-axis to the right indicates the percentage exchange of total number of exchangeable amide hydrogens. The solid lines are fits of a tri-exponential equation to the data to guide the eye. (**C**) Deuteron incorporation into full-length HtpG-E34A variant in the absence of nucleotides (open black circles) and in the presence of ATP (open red triangles). (**D**) Localization of fast and slow exchanging regions of nucleotide-free HtpG. Secondary structure representation of nucleotide-free HtpG (PDB ID code 2IOQ) with segments corresponding to peptic fragments coloured according to the relative deuteron incorporation into the nucleotide-free protein after 10 s (left panel) and 10 min (right panel) in D_2O as indicated in the figure. Numbers indicate segments mentioned in the text. NBD, nucleotide-binding domain; MD, middle domain; DD, dimerization domain. N and C terminus are indicated.

The ATPase cycle of HtpG

The issue, whether the highly protected state was an ATP-bound state or a post-hydrolysis state, could be resolved by determining the rate-limiting step of the ATPase cycle. To this end, we measured the ATPase rate constant of HtpG under steady state and single turnover conditions. The velocity of ATP hydrolysis of HtpG increased with increasing ATP concentrations, according to normal Michaelis–Menten kinetics, resulting in a k_{cat} of $0.011 \pm 0.001\ s^{-1}$ ($\tau = 90$ s) and a K_M of $250 \pm 82\ \mu M$ at 30°C (Supplementary Figure 1). Under single turnover conditions, the amount of ATP decreased with single exponential kinetics resulting in a hydrolysis rate constant k_{hyd} of $0.0077 \pm 0.0003\ s^{-1}$, which is smaller but close to the steady state ATPase rate constant. These results show that product release is not rate limiting in the ATPase cycle of HtpG. Therefore, in the presence of high concentrations of ATP, the majority of HtpG molecules is in the ATP-bound state.

As an independent confirmation of these results, we repeated the HX experiments in the presence of the non-hydrolysable ATP analogue AMPPNP, which was devoid of any detectable amounts of ATP (Figure 1B). Here, we also observed a strong protection of about 35 amide hydrogens as compared with 7 in the presence of ADP and 47 in the presence of ATP. Strikingly, in the presence of AMPPNP, we observed the same protection throughout the entire kinetics up to 3600 s incubation time, which contrasts with the loss of protection observed after 1200 s in the presence of ATP. We made the same observation when using an HtpG variant with Glu34 replaced by Ala (HtpG-E34A; constructed in analogy to the hydrolysis-deficient yeast Hsp82–E33A (Obermann *et al*, 1998; Panaretou *et al*, 1998)) (Figure 1C), which in our hands hydrolyses ATP ($\tau = 1071$ s) about 10-times more slowly than wild-type HtpG at 30°C. However, at very long time-points, the deuteron incorporation curve for HtpG-E34A in the presence of ATP also approaches the exchange curve for apo-HtpG-E34A (data not shown). These data indicate that the loss of protection in the presence of ATP is directly linked to ATP hydrolysis.

Taken together, our results show that (1) ATP hydrolysis is the rate-limiting step in the ATPase cycle of HtpG, (2) the ATP-bound state is the state with least solvent accessible amide hydrogens and (3) the ADP state shows only little protection as compared with the nucleotide-free state suggesting similar conformations. Henceforth, we call the most solvent protected ATP-bound state 'tensed (T) state' and the nucleotide-free state 'relaxed (R) state'.

Localization of fast and slow exchanging regions in nucleotide-free HtpG

To localize the regions within HtpG that contain slow and fast exchanging amide hydrogens, we digested the protein after the continuous-labelling HX reaction under quench conditions, using a column with immobilized pepsin in our HPLC setup as described previously (Rist *et al*, 2003). Such experiments allow the identification of structural elements in HtpG that are tightly folded in solution or that are in a rapid unfolding-refolding equilibrium.

The regularly observed peptic peptides of HtpG had an average length of 14.5 residues and covered 88% of HtpG's sequence (Supplementary Figure 2). Figure 1D shows secondary structure representations of apo-HtpG coloured according to the deuteration level of the analysed peptic fragments when the nucleotide-free protein was incubated for 10 s or 10 min in D_2O. Our HX data of HtpG free in solution are in good agreement with the published crystal structure of apo-HtpG (PDB entry code 2IOQ). Two exceptions are regions of the NBD that exhibited a high degree of solvent accessibility with almost complete deuteration within 10 s. These regions are the very N terminus (residues 2–19, all numbers in the text refer to the number of backbone amides within a peptide therefore omitting the first residue of the peptide, which does not contain an amide) and the so-called ATP-lid (residues 90–98 and 121–127; the ATP-lid was originally defined in yeast Hsp82 by Pearl and coworker as residues 95–125 (Prodromou *et al*, 1997a)). The crystal structure indicates a secondary structure with a significant number of hydrogen bonds for these regions (Figure 1D and Supplementary Figure 2). However, these regions have a relatively high b-factor denoting high degrees of positional variation consistent with our data.

Localization of nucleotide-induced changes in HtpG

To localize nucleotide-induced conformational changes, we compared deuteron incorporation into different segments of HtpG in the absence of nucleotide and in the presence of ADP, ATP and AMPPNP (Figure 2). The addition of ADP only had small effects on the incorporation of deuterons. For example, amide hydrogens were protected in the nucleotide-binding site (residues 90–98) and in the N-terminal segment (residues 2–19). In addition, a small but significant deprotection was detected in specific segments in the NBD (residues 108–119), the MD (residues 279–299 and 401–416) and almost the entire DD.

In the presence of ATP, we observed, in seven segments, a large protection (up to 7 amide hydrogens) compared with the nucleotide-free state (Figure 2A, middle panel; Figure 2B, dark blue segments): the N-terminal segments 2–19 and 21–31, the ATP-lid segments 90–98 and 121–127, the last helix of the NBD (residues 192–206) and the loop in the MD (residues 319–334 and 336–359) that contains the catalytic Arg336 (homologous to Arg380 in yeast Hsp82) (for detailed discussion see Supplementary data part 2). We detected a small but significant protection in additional segments scattered throughout the entire protein (Figure 2B, cyan segments). Two segments in the MD exhibited slightly more exchange in the presence of ATP than in the nucleotide-free state (Figure 2B, orange segments). Thus, our data show that ATP induces conformational changes not only in the NBD but throughout the HtpG protein leading to a significant loss of conformational dynamics.

The kinetics of deuteron incorporation in all of the highly protected segments in the presence of ATP were nearly identical with an average rate constant of $0.0038 \pm 0.0005\ s^{-1}$ (Figure 2B). This is fully consistent with ATP hydrolysis being rate limiting for HX in the ATP-bound state. As expected from the data for the full-length protein, the mutant protein, HtpG-E34A, exhibited a similar protection in the presence of ATP and this protection was observed over a much longer time interval (Figure 2B). Consistent with the hypothesis that ATP hydrolysis is rate limiting for HX, a bimodal distribution of the isotope peaks was observed in several peptides (Supplementary Figure 3). Bimodal isotopic peak distributions are indicative of the coexistence of two different conformational states. These two conformational states are the ATP-bound T state, in which the segments are

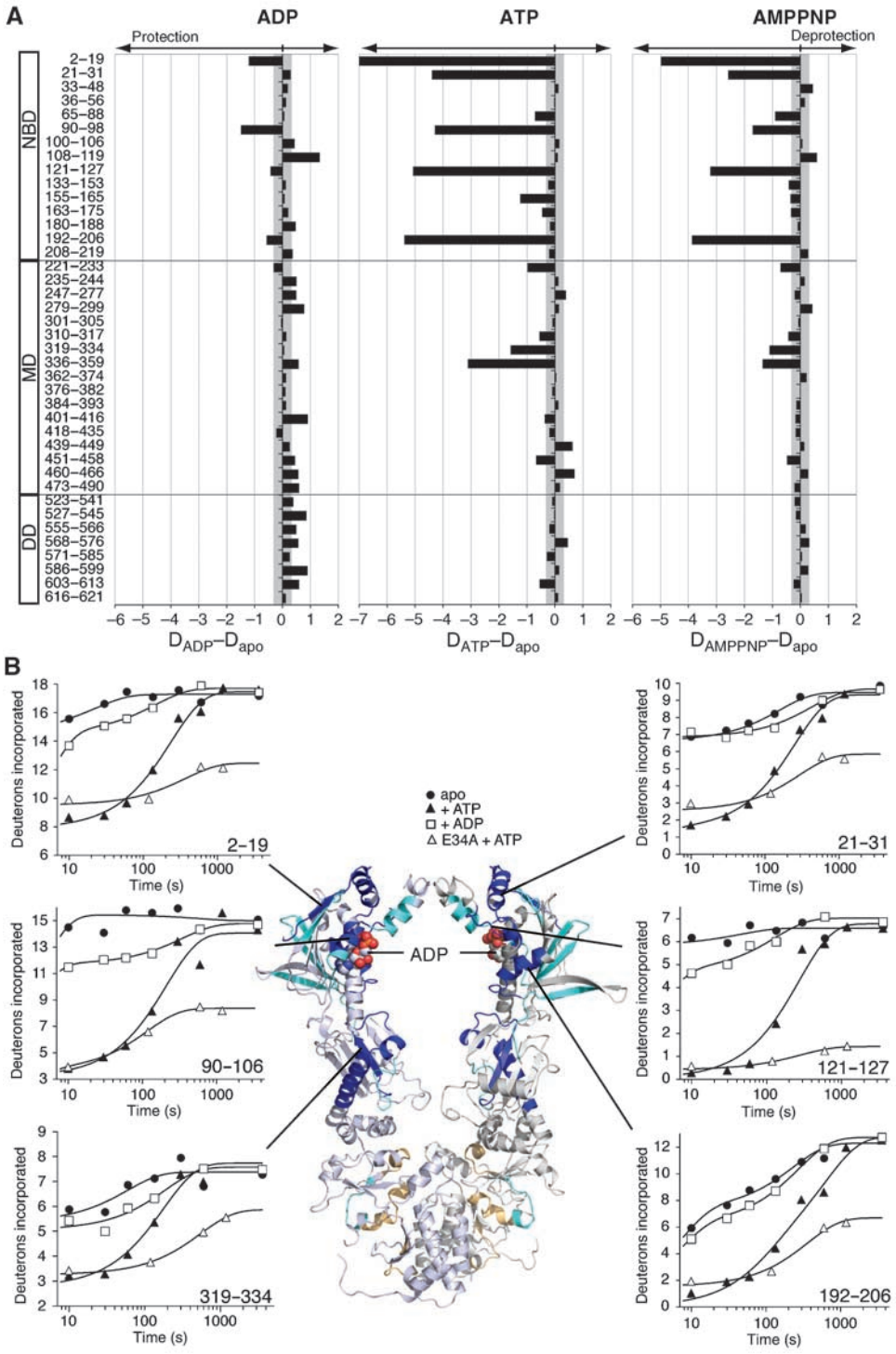

Figure 2 Nucleotide dependent changes in HtpG. (**A**) Difference plots of deuterons incorporated in the presence of ADP (left panel), ATP (middle panel) and AMPPNP (right panel) minus deuterons incorporated in the absence of nucleotides into HtpG segments after 30 s in D_2O. The domain structure of HtpG and numbers of the corresponding segments are given at the left of the panels. The data are the average of three independent experiments. The gray area indicates the average standard error. Bars within the gray area are not significantly different from zero. Bars to the left indicate nucleotide-induced protection, bars to the right indicate nucleotide-induced increase in solvent accessibility, that is, opening of the structure. (**B**) Nucleotide-dependent HX kinetics of selected segments of HtpG. Secondary structure representation of the crystal structure of full-length *E. coli* HtpG in complex with ADP (PDB ID code 2IOP; only one dimer shown with protomers in different shades of gray). Segments with more than 1.5 amide hydrogens protected in the presence of ATP at time-point 30 s are coloured in dark blue and the HX kinetics for these segments in the absence of nucleotides (black circles) and the presence of ADP (open squares) and ATP (black triangles) and for HtpG-E34A in the presence of ATP (open triangles) are shown. The solid lines are fits of a bi-exponential equation to the data to guide the eye. For this fit, the total amplitude was fixed to the total number of exchangeable amide hydrogens, and the rate constant for the first phase was estimated from the theoretical exchange rate constant in the unprotected peptide. Segments with 0.5 to 1.5 amide hydrogens protected at 30 s are coloured in cyan. Segments deprotected upon ATP binding are coloured in orange.

largely protected from HX, and the ADP-bound and nucleotide-free R state with higher HX rate constants.

In the presence of AMPPNP, the same changes in deuteron incorporation occurred as in the ATP-bound state, which confirms that the T state is the pre-hydrolysis state (Figure 2A). The magnitude of the observed protection was slightly reduced compared with the ATP-bound state, consistent with our HX data for full-length HtpG.

Some of the observed ATP-induced changes in amide hydrogen protection could be caused by an N-terminal dimerization, which was shown to occur in yeast Hsp82 upon ATP or AMPPNP binding (Prodromou *et al*, 2000; Ali *et al*, 2006). To test this hypothesis, we constructed a C-terminal truncation variant of HtpG (HtpGΔC containing residues 1–496), which lacks the DD and, consequently, is monomeric (Krukenberg *et al*, 2008). For reasons explained in detail below this truncation variant contained, in addition, the Glu12 to Cys amino acid replacement (HtpGΔC-E12C). This amino acid replacement did not change the conformational dynamics of the protein significantly as the full-length HtpG-E12C incorporated deuterons with the same kinetics as wild-type HtpG (data not shown). As verified by size exclusion chromatography in the absence or continuous presence of ATP and site-specific cross-linking HtpGΔC-E12C was monomeric independent of the nucleotide bound (Supplementary Figure 4 and data not shown). Comparison of deuteron incorporation into HtpGΔC-E12C in the presence or absence of ATP revealed the same degree of protection as observed for full-length HtpG, indicating that N-terminal dimerization is not responsible for the protection of amide hydrogens on addition of ATP (Supplementary Figure 5A). This result seems similar to the biochemical data for human Hsp90, the ATPase activity of which was shown not to be dependent on N-terminal dimerization (McLaughlin *et al*, 2004).

Taken together, significant nucleotide-dependent changes of the conformational dynamics of HtpG were observed in all three domains of the protein. Our data not only show the existence of an R and a T state but also show which structural elements of the protein are more tightly folded in the T state. This T state is not dependent on N-terminal dimerization because it can be reached in a monomeric truncation variant of HtpG.

Kinetics of R to T transition

As mentioned above, we noticed that the T state was only observed after a pre-incubation with ATP. To explore this observation in more detail, we measured the kinetics of R-to-T transition using pulse-labelling HX experiments as schematically illustrated in Figure 3A. HtpG and HtpG-E34A were incubated for different time intervals with ATP and then pulse-labelled for 10 s with D_2O. As the HX reaction times were always identical, changes in the numbers of incorporated deuterons are because of the ATP-induced transition from the R to the T state. In the absence of ATP or at the shortest time-point after addition of ATP, only a single mass peak is observed (Figure 3B and C). However, the mass of pulse-labelled HtpG after the shortest incubation with ATP was already smaller than the mass of pulse-labelled apo-HtpG, indicating a conformational transition that happens within 10 s. At later time-points, a second species with a still lower mass appeared and became dominant. These data strongly suggest a two-phase transition: a rapid transition

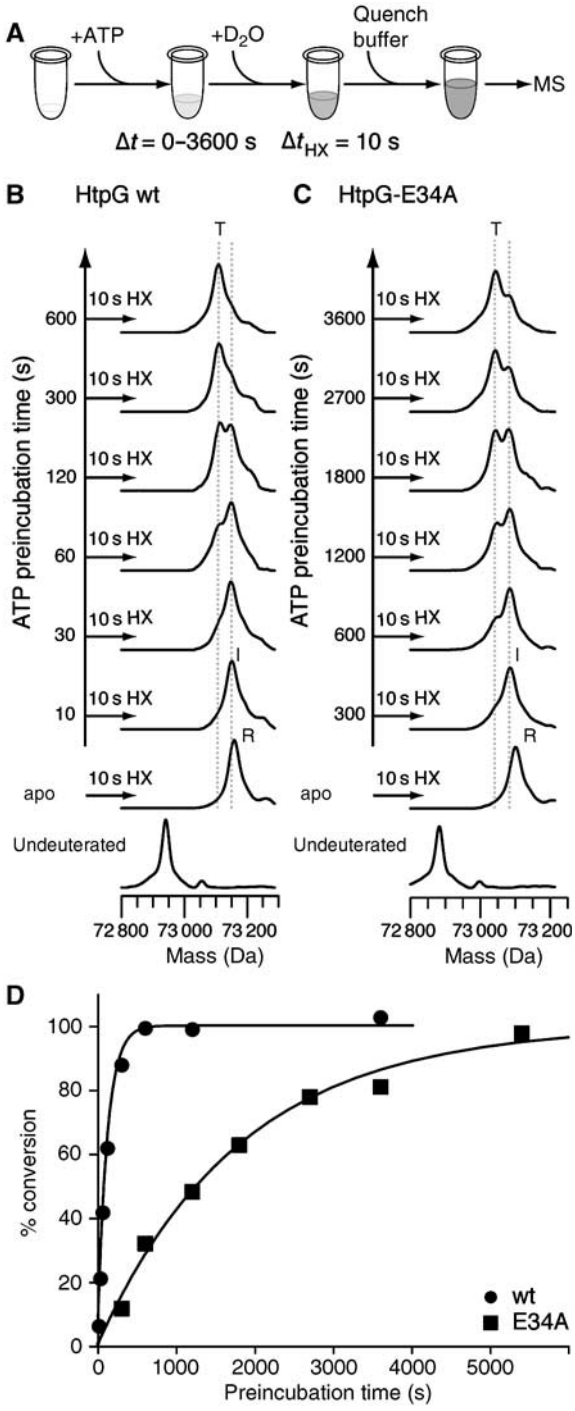

Figure 3 Kinetics of the ATP-induced R to T transition of HtpG. (**A**) Scheme of the experiment. (**B**, **C**) Deconvoluted mass spectra of wild-type HtpG (B) and HtpG-E34A (C) before incubation in D_2O (bottom curve), after 10 s in D_2O in the absence of nucleotides (apo; R state) or after different pre-incubation times with ATP (as indicated to the left; 10-fold different scale between A and B) followed by pulse-labelling for 10 s in D_2O. Dashed gray lines indicate the maximum of the mass peaks after 10 s pre-incubation in the presence of ATP (I state) and after 600 s (B) and 3600 s (C) pre-incubation in ATP (T state) as designated. The masses for R, I and T states were 73 158 ± 3, 73 151 ± 1 and 73 106 ± 1 for wild-type HtpG and 73 100 ± 3.5, 73 086 ± 3 and 73 046 ± 6 for HtpG-E34A, respectively. (**D**) Relative amount of T state versus the pre-incubation time in ATP. A first-order rate equation was fitted to the data (solid line) to give the I to T conversion rate constants of 0.01 s^{-1} and 0.0006 s^{-1} for wild-type HtpG and HtpG-E34A, respectively.

between the fast exchanging R state to a slightly protected intermediate (I) state and a subsequent slow transition to the considerably protected T state. The second transition is much slower in HtpG-E34A (Figure 3B, right panel). We fitted an equation for two Gaussian peaks to the data and determined the relative amount of I and T states (Figure 3D). The average I to T conversion rate constant for wild-type HtpG and mutant HtpG-E34A were 0.01 s^{-1} and 0.0006 s^{-1}, respectively, which are within the error of the experiment identical to the ATP hydrolysis rate constants showing that the conformational changes are rate-limiting for ATP hydrolysis under these conditions.

We also analysed the R to T transition for the monomeric HtpGΔC-E12C (Supplementary Figure 5B). Similar to the full-length proteins, the HtpGΔC-E12C converted rapidly into an I state on addition of ATP, and then very slowly into the T state. The rate constant for this conversion was much lower than for full-length HtpG, suggesting that the ATPase activity of this fragment is considerably lower than for the full-length protein as has been reported for the analogous fragment in yeast Hsp82 (Richter *et al*, 2001). Direct measurement of the ATPase rate constant for HtpGΔC-E12C yielded a value of 0.0018 s^{-1}, confirming this hypothesis.

Together, these data show that the R to T transition occurs in at least two steps with a first, fast step equilibrating within 10 s and a second, slow step, the rate constant of which is decreased dramatically either by the single amino acid replacement of Glu34 to Ala or by the elimination of dimerization.

Spatial resolution of the R to T transition

Our HX-MS data on peptide level revealed ATP-dependent conformational changes not only in regions close to the nucleotide-binding site but also in regions far distant in space. This raises the question of whether all ATP-induced conformational changes occur simultaneously in a concerted fashion or whether they occur in an ordered succession of events. In the first scenario, the protein would oscillate continuously between an open and a closed state with ATP-binding trapping the closed state. In the second scenario, ATP would bind to the open state and trigger local conformational

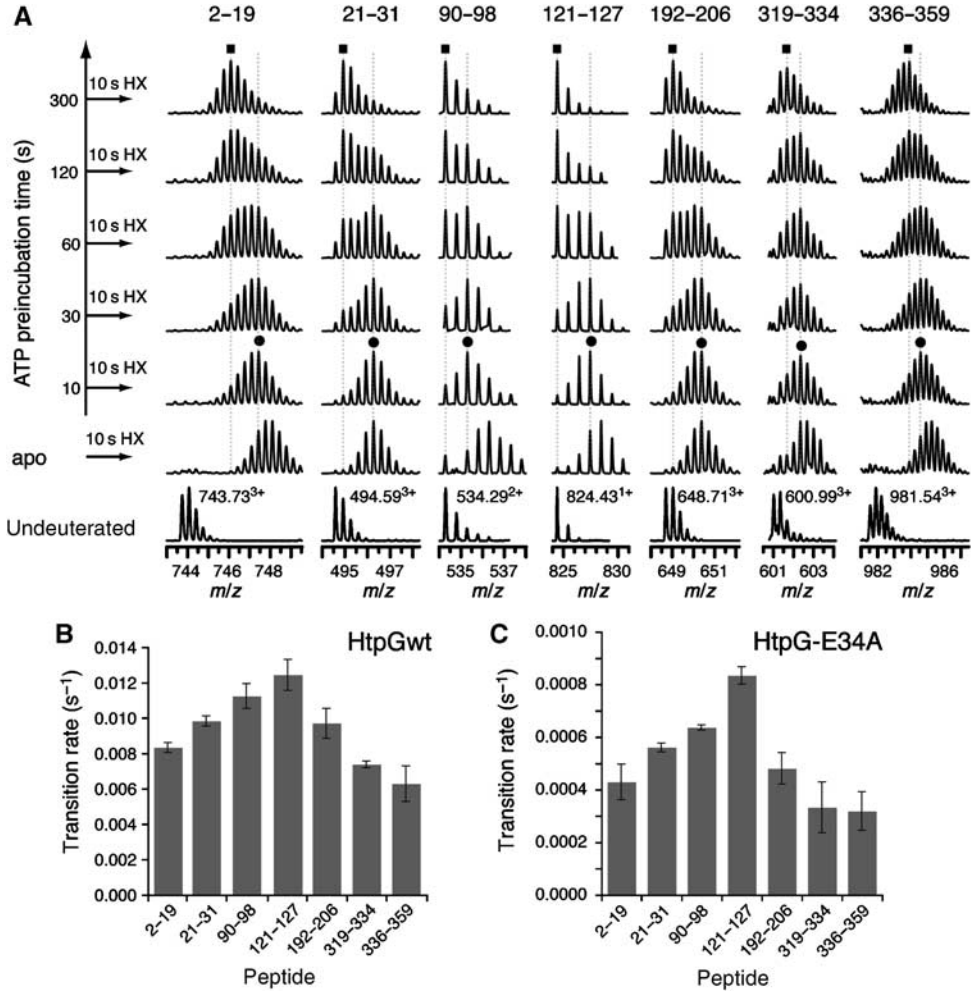

Figure 4 Spatially resolved kinetics of R to T transition. (**A**) Representative mass spectra (m/z scale) of selected peptic peptides of wild-type HtpG before incubation in D_2O (bottom curve; monoisotopic mass-to-charge ratio and charge state are given), after 10 s in D_2O in the absence of nucleotides (apo) or after pre-incubation for 10 to 300 s with ATP (as indicated to the left) followed by pulse-labelling for 10 s in D_2O. Dotted gray lines indicate the highest peak after 10 s pre-incubation in ATP followed by 10 s HX (I state, black circle) and the highest peak after 300 s pre-incubation in ATP followed by 10 s HX (T state, black square). The numbers above the spectra refer to the corresponding backbone amides. The actual peptic peptide contains one additional N-terminal residue. (**B**, **C**) I to T transition rate constants for selected peptides of wild-type HtpG (B) and HtpG-E34A (C) calculated as described in Materials and methods. The bars represent the mean of three independent determinations and standard error of mean.

changes that are subsequently propagated throughout the protein. To distinguish between these two scenarios, we performed spatially resolved pulse-labelling HX experiments by including peptic digestion under quench conditions.

The comparison of the mass spectra of selected peptic peptides of HtpG in the nucleotide-free state with 10 s of incubation with ATP already revealed a significant shift of the centre of the isotopic peak distribution towards lower m/z values most notably in peptides 90–98 and 121–127, and also in peptides 2–19 and 336–359 (Figure 4A). These data locate the conformational changes that lead to the I state. At subsequent time-points, the isotope peaks in most spectra formed a clear bimodal distribution showing the simultaneous presence of two HtpG states with different solvent accessibility. The more accessible state slowly converts into a more protected state. From the intensities of the highest peaks in the two states, we determined the rate constants for the I to T transition for each of the peptides analysed. It was interesting to note that the rate constant of I to T conversion was different in the analysed segments (Figure 4B). The transition rate constant was highest in the ATP-lid (segments 90–98 and 121–127) and decreased towards the N-terminal segment, 2–19, and the MD segments, 319–334 and 336–359, which contains the catalytic Arg336. For the HtpG-E34A variant protein, we observed the same phenomenon, although with overall much lower rate constants (Figure 4C and Supplementary Figure 6) as expected from the data for the I to T conversion of the full-length protein. However, the transition from the R to the I state occurred for HtpG-E34A, also within 10 s as a close analysis of the data for the earliest ATP pre-incubation time-points revealed. These data confirm that the R to T transition occurs in two phases: a fast phase, which cannot be resolved by HX, and a slow phase. As the first phase not only affects the ATP-lid region but also the N terminus and segments in the MD, it is a global transition to an intermediate state (I) that may happen in a concerted fashion. The major second phase, the transition from the I state to the T state, does not occur in all segments simultaneously but in sequential steps. The I to T conversion in the MD segments had the same rate constant as the single turnover ATPase rate constant, indicating that this conformational change is rate limiting for γ-phosphate cleavage.

Conformational changes in HtpG followed by fluorescence

To follow the kinetics of the conformational changes with better temporal resolution, we introduced a cysteine for fluorescent labelling at position 12 in HtpG, which is in the middle of a segment that strongly changes amide hydrogen accessibility on addition of ATP. HtpG-E12C was labelled with the environmental sensitive fluorophor, Hilyte Fluor™ 488 ($HtpG_{FL}$). The presence of ATP but not of ADP induced a time-dependent decrease in fluorescence (Figure 5A). Addition of a large excess of ADP to reactions of $HtpG_{FL}$, already equilibrated with ATP, led to an increase in fluorescence (Figure 5B). Close inspection of the fluorescence traces after the addition of ATP revealed that the fluorescence emission first increased rapidly before it decreased again (Figure 5A and B). We determined the kinetics of the first phase in the dependence of the ATP concentration using a stopped-flow device (Figure 5D and E). The observed rate constant increased with increasing ATP concentrations according to a hyperbolic relationship, which indicates a two-step process with a fast equilibrium as the first step and a subsequent isomerization. A fit of the hyperbolic equation to the data yielded a dissociation equilibrium constant of 3.6 ± 0.6 mM and forward and back isomerization rate constants of $227 \pm 12\ s^{-1}$ and $30 \pm 5\ s^{-1}$. The isomerization step was followed by the much slower conformational change, which caused the slow decrease in fluorescence. The rate constant for this step was determined from the traces of Figure 5A and B to $0.0089 \pm 0.0003\ s^{-1}$, which is very close to the I-to-T conversion rate constant of segment 2–19 as determined by HX-MS (Figure 4B). The reversion of the fluorescence decrease on addition of a large excess of ADP to the equilibrated reaction of $HtpG_{FL}$ with ATP occurs with a rate constant of $0.0062 \pm 0.0003\ s^{-1}$, which is similar to the ATP hydrolysis rate constant at the HtpG and ATP concentrations used. This argues that ATP hydrolysis is rate limiting for the fluorescence change and that ATP dissociation from this stage occurs at a rate constant of $\leqslant 0.0062\ s^{-1}$.

On addition of ADP to $HtpG_{FL}$, we also observed a rapid increase in fluorescence but no subsequent slow decrease. (Figure 5A and Supplementary Figure 7). These data are consistent with our HX-MS experiments, which revealed a small protection in segment 2–19 in the presence of ADP but not the large conformational change observed in the presence of ATP. From the dependence of the initial increase in fluorescence on the ADP concentration, we determined association and dissociation rate constants for ADP to be $70\,000 \pm 2300\ M^{-1}s^{-1}$ and $5.4 \pm 1.6\ s^{-1}$, respectively.

To better understand the cause for the ATP-dependent changes in fluorescence, we fluorescently labelled the cysteine containing monomeric C-terminal truncation fragment (HtpGΔC-E12C; $HtpG\Delta C_{FL}$). As for the dimeric full-length protein, addition of ATP led to a rapid increase in fluorescence (Figure 5A). However, the subsequent slow decrease could not be observed for $HtpG\Delta C_{FL}$, suggesting that N-terminal dimerization is responsible for the quench of fluorescence observed for full-length HtpG. More specifically, the interaction of the two fluorophors at the NBD seemed to be responsible for the quenching because a mixture of labelled and unlabelled HtpG exhibited, on addition of ATP, a smaller decrease of fluorescence than labelled HtpG alone (Figure 5A). In a 1:1 mixture of labelled and unlabelled HtpG, protomers exchange stochastically and only 25% of the dimers are homodimers of $HtpG_{FL}$.

As fluorescence could monitor ATP binding and subsequent isomerization steps, we extended our analysis to HtpG-E34A to determine which of these steps are affected by Glu34. On addition of ATP, the fluorescence first increased rapidly, as observed for the wild-type protein, but the subsequent decrease in the fluorescence was significantly slower (Figure 5C). The addition of excess ADP to the equilibrated reaction of HtpG-$E34A_{FL}$ with ATP led to the recovery of the fluorescence. From the kinetic analysis of the fast, first phase of the reaction, we determined the K_D for the association step to be 2.1 ± 1.2 mM and the forward isomerization rate constant to be $368 \pm 69\ s^{-1}$ (Figure 5E). The data did not yield a precise value for the back isomerization rate constant. The slow decrease in fluorescence as a consequence of N-terminal dimerization yielded a rate constant of $(8.3 \pm 0.2) \times 10^{-4}\ s^{-1}$, and the increase in fluorescence after addition of ADP to the HtpG-$E34A_{FL}$ ATP complex as a consequence of the replace-

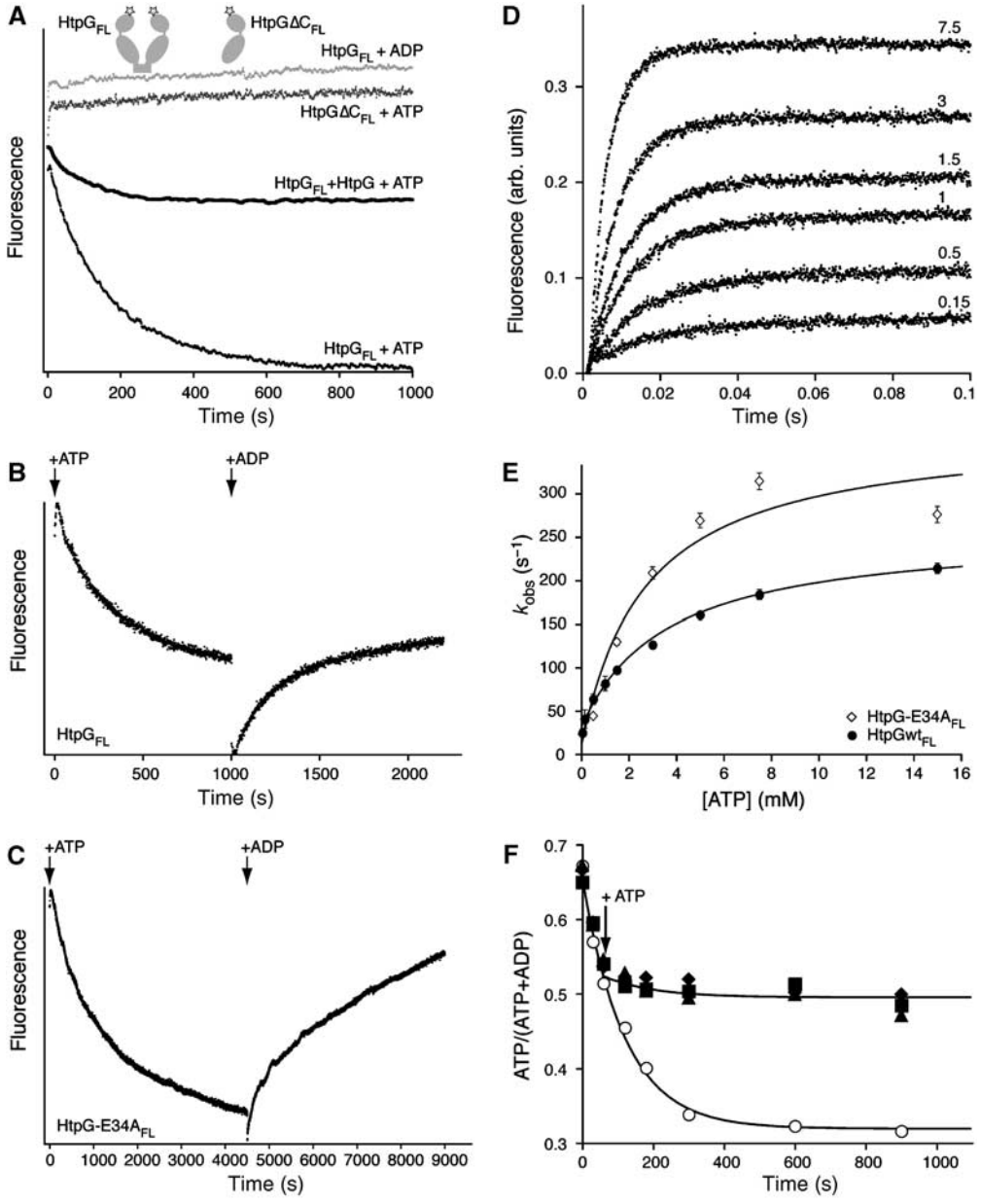

Figure 5 Kinetics of nucleotide-induced conformational changes followed by fluorescence. (**A**) Fluorescence trace of fluorescently labelled dimeric HtpG-E12C (HtpG$_{FL}$; 300 nM), HtpG$_{FL}$ (300 nM) mixed with unlabelled HtpG (600 nM), or monomeric HtpGΔC-E12C (HtpGΔC$_{FL}$, 300 nM) after addition of ADP (20 mM) or ATP (20 mM) as indicated (excitation 475 nm; emission 525 nm). For better visibility, the curves were shifted in *y*-axis direction. (**B**) Fluorescence trace of HtpG$_{FL}$ (300 nM) after addition of ATP (20 mM) and subsequent addition of ADP (40 mM) as indicated by the arrows. (**C**) Fluorescence trace of HtpG-E34A$_{FL}$ (300 nM) after addition of ATP (20 mM) and subsequent addition of ADP (40 mM) as indicated by the arrows. (**D**) Fluorescence traces of HtpG$_{FL}$ (150 nM final concentration) after rapid mixing 1:1 with 0.15 to 7.5 mM ATP (final concentrations) (excitation 488 nm; cut-off filter 530 nm). (**E**) Plot of the observed rate constants of fluorescence increase versus the ATP concentration. The solid line represents the non-linear regression fit of a hyperbolic equation giving a K_{D1} of 3.6 ± 0.6 mM, k_2 of 227 ± 12 s^{-1} and k_{-2} of 30 ± 5 s^{-1} (means of two independent determinations) for wild-type HtpG and a K_{D1} 2.1 ± 1.2 mM and k_2 of 368 ± 69 s^{-1} for HtpG-E34A (k_{-2} was not precise enough determined by the data). (**F**) Single-turnover ATPase assay to determine the degree of commitment to catalysis of bound ATP. HtpG (50 μM) was mixed with [α-^{32}P]ATP (40 μM; 3.7 kBq) and ATP hydrolysis followed by thin layer chromatography and phosphoimaging. The ratio of ATP divided by ATP plus ADP is plotted versus incubation time. At the indicated time-point 5 mM unlabelled ATP was added to the samples with filled symbols (three independent experiments shown); open circle, control sample. The solid lines are non-linear regression fits of a single exponential decay function to the data.

ment of ATP by ADP yielded a rate constant of $(2.6 \pm 0.4) \times 10^{-4}$ s^{-1}.

Taken together, our fluorescence experiments enabled us to dissect the ATPase cycle of HtpG (Figure 6A). The fluorescent probe monitored a series of nucleotide-dependent conformational changes in the segment 2–19, which are fully consistent with our HX-MS experiments. Thereby, we link conformational changes, as observed by HX-MS, and N-terminal dimerization to the kinetic parameters of the ATPase cycle. These data also clearly show that Glu34

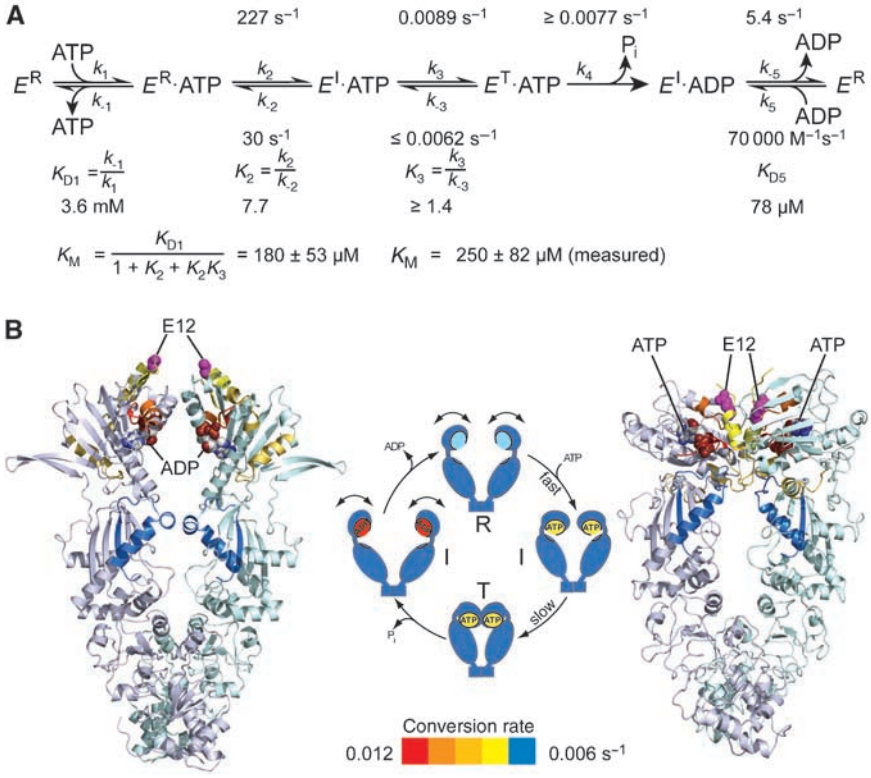

Figure 6 ATPase cycle of HtpG and model of conformational changes. (**A**) Steps of the ATPase cycle of HtpG with rate and equilibrium constants as determined by fluorescence spectroscopy and biochemical assays. E^R, E^I and E^T, HtpG in the relaxed, intermediate and tensed states. (**B**) Model of conformational changes of HtpG during the ATPase cycle. Secondary structure representations of the crystal structure of ADP-bound HtpG (PDB entry code 2IOP (Shiau *et al*, 2006); left panel) and of an homology model of HtpG on the crystal structure of yeast Hsp82 in complex with AMPPNP and Sba1 (PDB entry code 2CG9 (Peitsch, 1995, 1996; Guex and Peitsch, 1997; Ali *et al*, 2006)) as model for the ATP-bound structure of HtpG (right panel) coloured according to the I to T transition rate constants with red (high rate constants) to blue (low rate constants). Residue Glu12 (E12), where the fluorescent dye was attached in the HtpG-E12C variant, is shown in magenta. Between the structural representations, a model of the ATPase cycle is shown, which includes the nucleotide-free R state, the first intermediate (I state) after ATP binding, the T state and the ADP-bound state, which is similar to the I state.

only slows down the transition from the I to the T state and not the preceding steps of the ATPase cycle, i.e. ATP binding and R to I transition.

Commitment to catalysis

The fluorescence data showing that ATP displacement by ADP occurs at a rate constant similar to the ATP hydrolysis rate constant suggest that once the ATPase cycle has reached the T state, ATP is committed to catalysis. To test this hypothesis, we performed single turnover ATPase assays using [α-^{32}P]ATP (Figure 5F). At 60s after the start of the reaction we added an excess of unlabelled ATP to prevent rebinding of any dissociated [α-^{32}P]ATP. After addition of unlabelled ATP, conversion of [α-^{32}P]ATP into ADP did not stop immediately but continued with essentially the same rate constant, but the total amount of ATP that was converted decreased to 13% of the control sample. These data indicate that 13% of the ATP could not be replaced by cold ATP and was therefore committed to catalysis. Approximately the same fraction of HtpG molecules is converted into the T state under these conditions.

These data show that the last slow conformational change after the addition of ATP leads to trapping of ATP and commitment to catalysis.

Discussion

Our analysis of the conformational dynamics of the *E. coli* Hsp90 homologue, HtpG, yielded several novel insights into the ATPase cycle of HtpG: (1) Nucleotide binding induces conformational changes in NBD, MD and DD; (2) The ATP-bound state is the HtpG state with least backbone amide hydrogens solvent accessible; (3) The majority of the ATP-induced conformational changes happen surprisingly slowly and with different rate constants, with the highest rate constants in the nucleotide-binding pocket and decreasing rate constants towards the very N terminus and the MD; (4) The I to T conversion also occurs in a monomeric HtpG truncation variant, although much more slowly, showing that N-terminal dimerization accelerates this step; (5) Glu34 is important for the rate constant of I to T conversion but not for the rate constant of ATP binding or the R to I conversion; (6) The slow conformational change leads to trapping of the ATP and to commitment to catalysis; this step is rate limiting for ATP hydrolysis and therefore acts like a timer for the chaperone cycle of HtpG. In addition, our fluorescent probe allowed us to determine the kinetics of ATP binding, which occurs in a multi-step process.

Our data differ significantly from a recent HX-MS study on human Hsp90 (Phillips *et al*, 2007). In this study, Jackson and

coworkers analysed the influence of two inhibitors, which bind into the nucleotide-binding pocket, and of the cochaperone Cdc37 on the conformational flexibility of Hsp90. Although some of the inhibitor-induced changes in human Hsp90 occurred in similar regions as the ATP-induced changes in HtpG, the magnitude was much smaller, and it remains an open question whether inhibitors in general cause smaller changes than nucleotides or whether the human Hsp90 protein is less affected by ligand binding to the nucleotide-binding pocket.

A recent crystallographic and electronmicroscopic study provided evidence that HtpG performs dramatic conformational changes when progressing through the ATPase cycle (Shiau *et al*, 2006). In this study, the ADP-bound state was proposed to be the most compact conformation within the ATPase cycle of HtpG. Our data show that the ATP-bound state, and not the post-hydrolysis or the ADP-bound state is the least solvent accessible and the most rigid state of HtpG in solution. Although the ADP-bound state may have a more compact shape as proposed by Agard and coworkers (Shiau *et al*, 2006), it is nonetheless almost as flexible as the nucleotide-free state. Alternatively, a compact ADP-bound state exists only transiently. As HX-MS can detect coexisting conformations with different degrees of protection, a highly protected compact ADP state cannot constitute a major subpopulation. These conclusions are consistent with a recent SAXS study on HtpG (Krukenberg *et al*, 2008).

Our HX-MS and fluorescence data show that ATP binding induces a series of consecutive conformational states that are in equilibrium with each other (Figure 6A). ATP associates with the R-state of HtpG to form an initial encounter complex that has a dissociation equilibrium constant of 3.6 mM. The encounter complex is converted rapidly with a rate constant of $227\,s^{-1}$ into an intermediate state. A similar two-step binding process with very similar equilibrium and rate constants was also derived for human Hsp90 from steady state and pre-steady state kinetics (McLaughlin *et al*, 2004). The I state of HtpG is characterized by reduced solvent accessibility of backbone amide hydrogens in several regions of the protein, including segment 2–19 and segments in the MD, and an increase in fluorescence of a fluorophor at position 12. The transition to the I state occurs, most likely, in a concerted conformational change. ADP binding also induces a small protection in segment 2–19 (Figure 2) and a fluorescence increase of $HtpG_{FL}$ (Supplementary Figure 7). Thus, the ADP-bound state might be similar to the ATP-induced I state. However, the subsequent slow step to the T state only occurs upon binding of ATP. This conversion appears as a succession of conformational changes starting around the nucleotide-binding pocket, for which we measured the highest conversion rate constant, and progressing stepwise towards the N terminus and the catalytic loop of the MD, which reach the T state conformation with lower rate constants. This is the first time that such stepwise changes in the conformation of an Hsp90 protein could be spatially and temporally resolved. Such sequential conformational changes may be more common in proteins as a Φ-value analysis of the acetylcholine receptor (Purohit *et al*, 2007) and a cryoEM study of the chaperonin CCT (Rivenzon-Segal *et al*, 2005) came to a similar conclusion. However, in the case of CCT, the conformational changes were observed in different subunits and not within one polypeptide.

The differences in rate constants are highly statistically significant as determined by an ANOVA test ($P = 0.0002$) and were independently observed for wild-type HtpG and variant HtpG-E34A. For wild-type HtpG, the highest and lowest rate constants were $0.012\,s^{-1}$ and $0.006\,s^{-1}$, respectively. Consequently, the last conformational change occurs, on an average, more than a minute after the first conformational change. Such differences could be critical for client protein folding on HtpG. Peptidylprolyl isomerization, for example, occurs at a similar time scale (Fischer, 2000), other folding processes are generally faster. Such a timer may be critical for HtpG function.

As discussed in more detail in Supplementary data, our data are consistent with the ATPase cycle for yeast Hsp82 (Weikl *et al*, 2000; Richter *et al*, 2001) and the recently published data for mitochondrial Hsp90 Trap1 (Leskovar *et al*, 2008). In contrast to these publications, our data suggest that N-terminal dimerization precedes docking of NBD and MD.

Glu33 in Hsp82 was originally linked to catalysis of γ-phosphate cleavage because of the structural similarity to DNA gyrase B, in which the homologous Glu42 was shown to act as the general base (Jackson and Maxwell, 1993; Obermann *et al*, 1998; Panaretou *et al*, 1998). On the basis of our data (see also Supplementary data), we propose that Glu34 in HtpG has an additional role in coordinating the docking of the NBD with the MD and the NBD of the second protomer in the HtpG dimer by guiding Arg336 to the γ-phosphate and by favouring strand exchange through stabilizing helix 2.

In conclusion, by analysing HtpG, which appears to act without cochaperones, with HX-MS and fluorescence spectroscopy, we were able to establish the evolutionary basic ATPase cycle of Hsp90 proteins and to resolve the kinetics of conformational changes with an unprecedented spatial resolution. It will be interesting to observe how the conformational changes are conserved in the ATPase cycles of eukaryotic Hsp90 proteins, and how they are modulated by cochaperones and client proteins.

Materials and methods

Protein purification

HtpG, HtpG-E34A, HtpG-E12C, HtpG-E12C,E34A and HtpGΔC-E12C were expressed as C-terminal His_{10}-fusions in *E. coli* MC4100 Δ*htpG*::kan, and purified by Ni-IDA-chromatography (Protino, Macherey-Nagel) and anion-exchange chromatography (ResourceQ, GE Healthcare). The purified proteins were checked to be nucleotide-free by anion-exchange chromatography (ReSourceQ) and by UV detection by 254 nm.

ATPase assays

Single turnover assays were performed with 50 μM HtpG, 40 μM ATP and 3.7 kBq [α-^{32}P]ATP. At different time-points the reaction was quenched in 10% acetic acid containing 400 mM LiCl, and ATP was separated from ADP by thin layer chromatography and quantified by phosphoimaging, as described (Mayer *et al*, 1999).

Steady state ATPase activity was measured in an enzyme-coupled colorimetric assay using pyruvate kinase/lactate dehydrogenase as described earlier (Ali *et al*, 1993) (see also Supplementary data).

Hydrogen-exchange experiments

HX-MS experiments were performed similar to those described earlier (Rist *et al*, 2003, 2006).

For continuous HX labelling experiments, nucleotide-free HtpG proteins (40 μM) were pre-incubated with a large excess of buffered ATP (120 mM), ADP (60 mM) and AMPPNP (60 mM) for at least 10 min (90 min for HtpG-E34A) or with HKM buffer as control at 30°C to ensure that the steady-state equilibrium is reached. For pulsed HX labelling, the apo-proteins were pre-incubated with nucleotides or an equivalent amount of buffer for the indicated time intervals at 30°C before HX labelling was performed for 10 s.

Amide hydrogen exchange was initiated by a 20-fold dilution of the proteins into D_2O buffer containing 25 mM HEPES, pD 7.4, 50 mM KCl and 5 mM $MgCl_2$ at 30°C. After various time intervals (10 s–90 min), the exchange reaction was quenched by decreasing the temperature to 0°C and the pH with ice-cold quench buffer (400 mM KH_2PO_4/H_3PO_4, pH 2.2). Quenched samples were directly injected into an HPLC-MS setup as described (Rist *et al*, 2003, 2005) (see also Supplementary data).

Analysis of HX kinetics

Analysis of HX experiments was performed essentially as described earlier (Rist *et al*, 2003, 2006). For the kinetic analysis of the transition of I to T state in HX experiments, full length protein mass spectra of three independent measurements of 8 time-points were deconvoluted using MagTran software (Zhang and Smith, 1993), and the abundance of the two deuterated mass species was calculated by fitting two Gaussian peaks with different means and areas but with similar width into the deconvoluted spectra using the following equation:

$$y = \frac{A_1}{\sigma\sqrt{2\pi}} e^{-\frac{1}{2}\left(\frac{x-\bar{x}_1}{\sigma}\right)^2} + \frac{A_2}{\sigma\sqrt{2\pi}} e^{-\frac{1}{2}\left(\frac{x-\bar{x}_2}{\sigma}\right)^2}$$

with A_1, A_2, $\bar{x}_1$ and $\bar{x}_2$ being the area and the mean of the first and second peak and σ being the standard deviation of the Gaussian peaks. The ratio of A_1 and the sum of A_1 and A_2 represented the relative amount of the T state. The absolute amount of I and T state at the shortest and longest time-points could not be assessed because of the tailing of the peaks to higher and lower mass range but were estimated from peptide data. The increasing amount of the T state in dependence of time was fitted using a first-order rate equation.

For the analysis of the transition kinetics in deuterated peptides, peptide MS spectra of three independent experiments with 10 different pre-incubation times were extracted, normalized to the highest peak of the isotope cluster and the intensity of two peaks determined (indicated with a circle and a square in Figure 4A): the peak, which is highest at 10 s pre-incubation with ATP (I state), and the peak, which is highest at 300 s pre-incubation with ATP (T state). We plotted the T state peak intensity divided by the sum of the intensities of the two peaks (T/(T + I)) versus time. This ratio followed first-order rate kinetics as determined by non-linear regression analysis using GraphPad Prism software.

Fluorescent labelling

Protein solutions of HtpG-E12C, HtpG-E12C-E34A and HtpGΔC-E12C were reduced with 10 mM TCEP and then incubated with Hilyte Fluor™ 488-C2-maleimide (AnaSpec. Inc.) (dissolved in dimethylformamide) at room temperature for 1 hour. Unreacted label was blocked by the addition of 10 mM mercaptoethanol, and removed by desalting with a self-packed Sephadex-G-75 column (GE Healthcare) equilibrated in HKM buffer. The labelling efficiency was checked to be 100% by MS.

Fluorescence spectroscopy

Fluorescently labelled proteins $HtpG_{FL}$, HtpG-E34A_{FL} and HtpGΔC_{FL} were analysed at a concentration of 300 nM in HKM buffer. Fluorescence emission spectra were recorded in the absence or presence of ATP and ADP (20 mM final concentration) from 500 to 700 nm at an excitation wavelength of 475 nm on a Perkin Elmer LS-55 Luminescence Spectrometer at 30°C. The fluorescence at 525 nm was measured after addition of nucleotides in a time-course experiment over 20 min or 60 min for $HtpG_{FL}$ or the HtpG-E34A_{FL}, respectively. The data were fitted using GraphPad Prism software.

Stopped-flow analysis

Using a stopped-flow device (SX-18 M Applied Photophysics, Surrey, UK) $HtpG_{FL}$ (300 nM) in HKM buffer was rapidly mixed at a ratio of 1:1 with a solution of 0.003 to 30 mM ATP or ADP. Fluorescence (excitation 488 nm; cut-off filter at 530 nm) was measured for 0.1 to 10 s at 30°C. An exponential function was fitted to the time-dependent fluorescence increase using GraphPad Prism software.

Supplementary data

Supplementary data are available at *The EMBO Journal* Online (http://www.embojournal.org).

Acknowledgements

We thank Z Zhang for providing the program MagTran and HXPep, T Ruppert for his support in the mass spectrometry facility and B Bukau and D Huber for their comments on the manuscript. This work was supported by the Deutsche Forschungsgemeinschaft (SFB638).

References

Ali JA, Jackson AP, Howells AJ, Maxwell A (1993) The 43-kilodalton N-terminal fragment of the DNA gyrase B protein hydrolyzes ATP and binds coumarin drugs. *Biochemistry* **32:** 2717–2724

Ali MM, Roe SM, Vaughan CK, Meyer P, Panaretou B, Piper PW, Prodromou C, Pearl LH (2006) Crystal structure of an Hsp90-nucleotide-p23/Sba1 closed chaperone complex. *Nature* **440:** 1013–1017

Cunningham CN, Krukenberg KA, Agard DA (2008) Intra- and intermonomer interactions are required to synergistically facilitate ATP hydrolysis in Hsp90. *J Biol Chem* **283:** 21170–21178

Fischer G (2000) Chemical aspects of peptide bond isomerisation. *Chem Soc Rev* **29:** 119–127

Guex N, Peitsch MC (1997) SWISS-MODEL and the Swiss-PdbViewer: an environment for comparative protein modelling. *Electrophoresis* **18:** 2714–2723

Harris SF, Shiau AK, Agard DA (2004) The crystal structure of the carboxy-terminal dimerization domain of htpG, the Escherichia coli Hsp90, reveals a potential substrate binding site. *Structure* **12:** 1087–1097

Huai Q, Wang H, Liu Y, Kim HY, Toft D, Ke H (2005) Structures of the N-terminal and middle domains of E. coli Hsp90 and conformation changes upon ADP binding. *Structure* **13:** 579–590

Immormino RM, Dollins DE, Shaffer PL, Soldano KL, Walker MA, Gewirth DT (2004) Ligand-induced conformational shift in the N-terminal domain of GRP94, an Hsp90 chaperone. *J Biol Chem* **279:** 46162–46171

Jackson AP, Maxwell A (1993) Identifying the catalytic residue of the ATPase reaction of DNA gyrase. *Proc Natl Acad Sci USA* **90:** 11232–11236

Krukenberg KA, Forster F, Rice LM, Sali A, Agard DA (2008) Multiple conformations of E. coli Hsp90 in solution: insights into the conformational dynamics of Hsp90. *Structure* **16:** 755–765

Leskovar A, Wegele H, Werbeck ND, Buchner J, Reinstein J (2008) The ATPase cycle of the mitochondrial Hsp90 analog Trap1. *J Biol Chem* **283:** 11677–11688

Mayer MP, Bukau B (1999) Molecular chaperones: the busy life of Hsp90. *Curr Biol* **9:** R322–R325

Mayer MP, Laufen T, Paal K, McCarty JS, Bukau B (1999) Investigation of the interaction between DnaK and DnaJ by surface plasmon resonance spectroscopy. *J Mol Biol* **289:** 1131–1144

McLaughlin SH, Ventouras LA, Lobbezoo B, Jackson SE (2004) Independent ATPase activity of Hsp90 subunits creates a flexible assembly platform. *J Mol Biol* **344:** 813–826

Meyer P, Prodromou C, Hu B, Vaughan C, Roe SM, Panaretou B, Piper PW, Pearl LH (2003) Structural and functional analysis of the middle segment of hsp90. Implications for ATP hydrolysis and client protein and cochaperone interactions. *Mol Cell* **11:** 647–658

Obermann WM, Sondermann H, Russo AA, Pavletich NP, Hartl FU (1998) *In vivo* function of Hsp90 is dependent on ATP binding and ATP hydrolysis. *J Cell Biol* **143:** 901–910

Panaretou B, Prodromou C, Roe SM, O'Brien R, Ladbury JE, Piper PW, Pearl LH (1998) ATP binding and hydrolysis are essential to the function of the Hsp90 molecular chaperone *in vivo*. *EMBO J* **17:** 4829–4836

Pearl LH, Prodromou C (2002) Structure, function, and mechanism of the Hsp90 molecular chaperone. *Adv Protein Chem* **59:** 157–186

Pearl LH, Prodromou C (2006) Structure and mechanism of the hsp90 molecular chaperone machinery. *Annu Rev Biochem* **75:** 271–294

Pearl LH, Prodromou C, Workman P (2008) The Hsp90 molecular chaperone: an open and shut case for treatment. *Biochem J* **410:** 439–453

Peitsch MC (1995) Protein modeling by E-mail. *Biotechnology* **13:** 658–660

Peitsch MC (1996) ProMod and Swiss-Model: Internet-based tools for automated comparative protein modelling. *Biochem Soc Trans* **24:** 274–279

Phillips JJ, Yao ZP, Zhang W, McLaughlin S, Laue ED, Robinson CV, Jackson SE (2007) Conformational dynamics of the molecular chaperone Hsp90 in complexes with a co-chaperone and anticancer drugs. *J Mol Biol* **372:** 1189–1203

Prodromou C, Panaretou B, Chohan S, Siligardi G, O'Brien R, Ladbury JE, Roe SM, Piper PW, Pearl LH (2000) The ATPase cycle of Hsp90 drives a molecular 'clamp' via transient dimerization of the N-terminal domains. *EMBO J* **19:** 4383–4392

Prodromou C, Roe SM, O'Brien R, Ladbury JE, Piper PW, Pearl LH (1997a) Identification and structural characterization of the ATP/ADP-binding site in the Hsp90 molecular chaperone. *Cell* **90:** 65–75

Prodromou C, Roe SM, Piper PW, Pearl LH (1997b) A molecular clamp in the crystal structure of the N-terminal domain of the yeast Hsp90 chaperone. *Nat Struct Biol* **4:** 477–482

Purohit P, Mitra A, Auerbach A (2007) A stepwise mechanism for acetylcholine receptor channel gating. *Nature* **446:** 930–933

Richter K, Muschler P, Hainzl O, Buchner J (2001) Coordinated ATP hydrolysis by the Hsp90 dimer. *J Biol Chem* **276:** 33689–33696

Richter K, Reinstein J, Buchner J (2002) N-terminal residues regulate the catalytic efficiency of the Hsp90 ATPase cycle. *J Biol Chem* **277:** 44905–44910

Rist W, Graf C, Bukau B, Mayer MP (2006) Amide hydrogen exchange reveals conformational changes in hsp70 chaperones important for allosteric regulation. *J Biol Chem* **281:** 16493–16501

Rist W, Jørgensen TJD, Roepstorff P, Bukau B, Mayer MP (2003) Mapping temperature-induced conformational changes in the Escherichia coli heat shock transcription factor sigma 32 by amide hydrogen exchange. *J Biol Chem* **278:** 51415–51421

Rist W, Mayer MP, Andersen JS, Roepstorff P, Jorgensen TJ (2005) Rapid desalting of protein samples for on-line microflow electrospray ionization mass spectrometry. *Anal Biochem* **342:** 160–162

Rivenzon-Segal D, Wolf SG, Shimon L, Willison KR, Horovitz A (2005) Sequential ATP-induced allosteric transitions of the cytoplasmic chaperonin containing TCP-1 revealed by EM analysis. *Nat Struct Mol Biol* **12:** 233–237

Shiau AK, Harris SF, Southworth DR, Agard DA (2006) Structural analysis of E. coli hsp90 reveals dramatic nucleotide-dependent conformational rearrangements. *Cell* **127:** 329–340

Stebbins CE, Russo AA, Schneider C, Rosen N, Hartl FU, Pavletich NP (1997) Crystal structure of an Hsp90-geldanamycin complex: targeting of a protein chaperone by an antitumor agent. *Cell* **89:** 239–250

Vaughan CK, Piper PW, Pearl LH, Prodromou C (2009) A common conformationally coupled ATPase mechanism for yeast and human cytoplasmic HSP90s. *FEBS J* **276:** 199–209

Wegele H, Muller L, Buchner J (2004) Hsp70 and Hsp90-a relay team for protein folding. *Rev Physiol Biochem Pharmacol* **151:** 1–44

Weikl T, Muschler P, Richter K, Veit T, Reinstein J, Buchner J (2000) C-terminal regions of Hsp90 are important for trapping the nucleotide during the ATPase cycle. *J Mol Biol* **303:** 583–592

Zhang Z, Smith DL (1993) Determination of amide hydrogen exchange by mass spectrometry: a new tool for protein structure elucidation. *Protein Sci* **2:** 522–531